Foamed cementitious composites with 3D-printed auxetic lattice reinforcement enhancing static and cyclic performance

Meng, Zhaozheng; Xu, Yading; Zhou, Wen; Xie, Jinbao; Šavija, Branko

DOI
10.1016/j.compositesb.2025.112614

Publication date
2025

Document Version
Final published version

Published in
Composites Part B: Engineering

Composites Part B 303 (2025) 112614

Contents lists available at ScienceDirect

Composites Part B

journal homepage: www.elsevier.com/locate/compositesb

Foamed cementitious composites with 3D-printed auxetic lattice reinforcement: enhancing static and cyclic performance

Zhaozheng Meng [a,*], Yading Xu [a,b], Wen Zhou [a], Jinbao Xie [a], Branko Šavija [a]

[a] Microlab, Faculty of Civil Engineering and Geosciences, Delft University of Technology, Stevinweg 1, 2628 CN, Delft, the Netherlands
[b] College of Materials Science and Engineering, Chongqing University, Chongqing, 400045, China

ARTICLE INFO

Handling Editor: Dr Uday Vaidya

Keywords:
Foamed cementitious composites
Auxetic lattice
3D printing
X-ray CT
Cyclic loading

ABSTRACT

This study develops a novel class of 3D-printed auxetic lattice reinforced foamed cementitious composites, aimed at overcoming the brittleness and low strength of conventional foamed cement while maintaining lightweight characteristic. Polymeric auxetic lattices (mechanical metamaterials with negative Poisson's ratio) were 3D printed and embedded in foamed cement matrix. Static and cyclic compression tests were conducted to evaluate load-bearing capacity, energy absorption, and failure mechanisms. X-ray computed tomography (CT) analysis was performed to examine interfacial behavior between the lattice and cement matrix. Results indicate that 3D auxetic lattices significantly enhance strength and ductility through multidirectional lateral confinement, where the energy absorption increased by up to 2.8 times compared to unreinforced foamed cement at a density of 550 kg/m^3. Specifically, the 3D auxetic lattices reinforced composites showed pronounced resilience under cyclic loading, exhibiting gradual and ductile damage evolution while sustaining performance beyond 700 cycles. In comparison, 2D auxetic lattices which provide negative Poisson's ratio only in-plane are less effective in reinforcing foamed cement matrix. Additionally, although non-auxetic lattice increased load-carrying capacity to some degree, the corresponding composites structure showed localized shear failure and premature structural degradation under cyclic loading. Overall, the active reinforcement effect of auxetic lattices enables the development of advanced foamed cementitious composites for impact mitigation, blast protection, and buoyant components requiring energy absorption and repeated-load resilience.

1. Introduction

Lightweight cementitious materials have attracted significant attention due to their excellent engineering properties, which make them well-suited for various non-structural applications including acoustic insulation [1], cavity filling [2], and shock waves attenuation [3]. Among these materials, foamed cement paste has emerged as one of the most widely used lightweight construction solutions, as it can be manufactured with tailorable density and strength by controlling the foam dosage [4–6]. In addition, because of the low cement consumption, foamed cement can also contribute to the sustainable future of construction and built environments [7,8]. Despite these advantages, foamed cement paste often suffers from its limited strength, showing softening and even brittle behaviors particularly under high strain-rate cyclic or impact loading, where fragmentation failure will occur [9–11]. This damage susceptibility makes it extremely vulnerable to repeated events or aftershocks, effectively limiting its usability and sustainability in demanding scenarios. Consequently, improving mechanical performance through composite material strategies offers new opportunities for creating high-performance lightweight cementitious materials [12,13].

One of the commonly used strategies to increase the strength and ductility of foamed cementitious materials is to include fibers and using silica fume during the mixing process [14,15]. Gencel et al. [16] designed high-performance foamed concrete using basalt fibers and silica fume, but reported that the effect of basalt fibers is more dependent on the dosage of silica fume, and a 10 % increase in compressive strength was observed compared to specimens without fiber. Ahmad and Chen [17] also reported that adding silica fume would reduce the sorptivity and porosity of foamed concrete. Wang et al. [18] found that coir fibers (0.3 %) can contribute to an 42.19 % improvement in compressive strength. Falliano et al. [19] reported that the influence of short polymer fibers on compressive strength was negligible, while the improvement of flexural strength was quite significant. This limited role

* Corresponding author.
E-mail address: z.meng@tudelft.nl (Z. Meng).

https://doi.org/10.1016/j.compositesb.2025.112614
Received 12 March 2025; Received in revised form 8 May 2025; Accepted 9 May 2025
Available online 11 May 2025

of fibers in compression is mainly due to the complex interactions between the fibers and the highly porous matrix. Amran et al. [20] concluded that factors such as elastic modulus, fiber length, fiber dosage, and the volume of the entrapped air bubbles all influence the compressive strength and toughness of foamed concrete. To achieve better properties, foam concrete sometimes requires curing in autoclave (high temperature and high pressure environment) which consumes a large amount of energy. Kilincarslan et al. [21] tested autoclaved aerated foam concrete and reported a maximum 443 % increase in compressive strength, and the thermal conductivity coefficients showed reductions compared to air cured specimens. Moreover, Nguyen et al. [22] fabricated buoyant foamed concrete by creating 3D-printed polylactic acid (PLA) shell molds and casting foamed concrete within them, demonstrating that the loading capacity of the resulting composites could be controlled by the molds' geometry.

With the recent development of additive manufacturing technology, 3D-printed reinforcement has emerged as a promising solution for reinforcing materials [23,24]. Benefiting from the design flexibility of 3D printing, the mechanical properties of these composites can be engineered by tuning the architecture of the printed reinforcement [25,26]. Among the various structural designs of 3D-printed reinforcement, auxetic lattices exhibiting a negative Poisson's ratio have attracted considerable attention due to their unique ability to contract laterally when compressed [27–29]. Classical auxetic metamaterials mainly include re-entrant structures [30], rotating structures [31], chiral structures [32], polymer foams [33], and some other variants [34,35]. The auxetic behavior gives rise to a number of advantages which have been exploited in applications ranging from biomedical implants to impact-resistant composites [36]. Benefited from the large deformation capacity and sensitivity to external stress, auxetic materials are often used as components of soft robots [37]. Furthermore, due to its contraction nature under compression and the induced biaxial compression effect [38], the auxetic composite could show three times larger indentation stiffness and two times higher energy absorption capacity compare to the non-auxetic composite [39].

In the context of cementitious materials, the lateral contraction from auxetic behavior can actively confine cement matrix, thereby enhancing the energy absorption, toughness, and damage tolerance of cement-based materials, making auxetic lattices an attractive option for creating more resilient composite structures [39–41]. For example, Zahra et al. created auxetic foam composites using auxetic foam as protective layers for impact protection [33,42]. Recent studies on auxetic lattice reinforced normal-weight concrete also confirmed that the auxetic lattice reinforcement can significantly improve the ductility, energy absorption capacities, and crack controlling [43–45]. Some researchers also reported that by using metallic auxetic lattices, the peak and residual strength can also be significantly improved [46,47].

Despite these promising advancements, most existing research on 3D-printed auxetic lattice reinforcement has focused on normal-weight concrete systems, where the comparatively weaker polymeric lattice may cause a reduction in the composite peak strength and stiffness compared to the reference (i.e., unreinforced concrete) [48]. In contrast, foamed cement-based material has a lower strength and stiffness due to its highly porous structure, which may allow the auxetic lattice to provide more effective confinement on the matrix. Furthermore, the interaction between the auxetic lattice and the foamed cement's porous microstructure remains largely unexplored. The foamed cementitious matrix's compactable nature and reduced density could potentially alter the manner in which auxetic lattice interacts with the surrounding matrix. Therefore, to better understand the reinforcing mechanisms of auxetic lattices in foamed cement matrices, more studies need to be carried out to guide the design of more resilient foamed cementitious composites.

In this study, an experimental and microstructural investigation was conducted to analyze how 3D-printed auxetic lattice reinforcements influence the mechanical performance of foamed cementitious composites. Specifically, 3D auxetic lattices showing negative Poisson's ratios in multiple directions, 2D auxetic lattices with negative Poisson's ratios only in-plane, and non-auxetic lattices were 3D-printed and embedded into the foamed cement matrix. Static compression tests were carried out to evaluate strength, ductility, and energy absorption, while cyclic loading experiments provided insights into fatigue resistance and damage evolution. In addition, X-ray computed tomography (CT) analysis was employed to capture the internal damage patterns and analyze the microstructural interaction between lattice reinforcement and foamed cement matrix.

The contributions from this study can be summarized in the following aspects. First, considering the difficulty in obtaining significant strength improvement for foam concrete while maintaining the low-density nature, this study demonstrates for the first time that utilizing 3D-printed auxetic lattices in foamed cement matrices can enhance compressive strength and post-peak ductility without sacrificing lightweight characteristics, which can offer a new and effective reinforcement solution to lightweight cementitious material. Second, it proved that the polymer-based auxetic lattices can be a good match for the low density cementitious matrix, where the auxetic lattices can transform the typical brittle failure of foamed cement into a stable and ductile mode, widening the application prospect of auxetic cementitious composites. Third, to better understand reinforcing mechanisms of auxetic lattice in lightweight cementitious materials, the interaction mechanisms between relative stiffness of foamed cement matrix and Poisson's ratio of the polymer lattice are systematically investigated and related to the composite's mechanical performance. It is revealed that not only the Poisson's ratio but also the matrix stiffness could influence the confinement effectiveness of the embedded reinforcement, highlighting the necessity of co-designing matrix properties and auxetic architecture to achieve the optimal performance in the field of cementitious composites. These contributions suggest that auxetic-reinforced foamed cementitious materials have strong potential in protective applications such as arrest systems, blast shielding, and impact-resistant barriers where not only energy absorption is needed but also post-impact functionality remains critical. Additionally, their lower density compared to water enables buoyant applications for resisting wave impact, as well as protections from vessel collisions and extreme weather events.

2. Experiments

2.1. Materials

CEM I 42.5 N Portland cement was used as the raw material to manufacture foamed cement paste. The Schuim 80/23 manufactured by Demula was used as synthetic foaming agent, and it should be mixed with water at a volume ratio of 0.03 to achieve a foaming ratio of 20 (i.e., generating 20 L foams when mixed with 1 L of water). The density of the foaming agent is 1060 kg/m^3.

In terms of 3D printed lattice reinforcements, recent studies showed that base materials used to manufacture auxetic materials can also influence the mechanical properties and isotropy [49–51]. In this study, the Henkel Loctite 3D IND405 HDT50 High Elongation resin was utilized as the base material. Its high elongation capacity ensures the printed lattice can undergo large joint deformation needed for auxetic behavior without cracking, while its stiffness provides sufficient resistance to compressive loads to actively confine the foamed-cement matrix. According to the tensile test results [48], the tensile stress at break is around 43.9 MPa, and the maximum elongation capacity could reach 62.5 %, and the Young's modulus is 1.7 GPa. The lattice reinforcement was 3D printed by the stereolithography technique where the resin was selectively polymerized by the ultraviolet light layer by layer. The printing and post-processing parameters used in this study can be found in Table 1.

Table 1
Printing parameters for the photosensitive resin.

Layer thickness	Normal layer exposure time	Bottom layer exposure time	Bottom layer numbers	Light-off delay (s)	Post-processing
50 μm	12 s	35 s	8	6.5 s	405 nm UV light for 5 min

Table 2
Mixture proportions of foamed cementitious matrix.

Cement paste		Foam		Wet density (kg/m^3)	Dry density (kg/m^3)
Water (g)	Cement power (g)	Water (g)	Foam agent (g)		
100	400	100	3.2	500	400
143.3	400	56.6	1.8	620	550
184.3	400	15.7	0.5	760	700

2.2. Preparation of auxetic foamed cementitious composites

The geometrical design of the auxetic and non-auxetic lattice reinforcements is displayed in Fig. 1. The 3D auxetic lattice was designed based on the concept of "rotating square" auxetic architecture, and the solid square was replaced by diagonal struts to ensure the infiltration of foamed cement matrix. The detailed design procedure of the 3D auxetic lattice structure can be found in our previous work [48]. The non-auxetic octet structure was included for comparison of the influence of auxetic behavior on the mechanical properties of auxetic foamed cementitious composites. The octet structure was selected because it shows a distinctly positive Poisson's ratio over the entire loading range, making it a suitable reference to contrast with auxetic lattices that exhibit negative Poisson's ratios. In addition, the Octet and the 3D auxetic lattice have comparable total strut length, so both can be printed with similar lattice volume using a similar strut diameter. This can avoid introducing other possible influencing variables such as buckling slenderness that could affect the Poisson-ratio effect. In addition, a two-dimensional auxetic lattice (only showing negative Poisson's ratio on the planar directions) structure was also included [52], to compare the influence of auxetic directions on the composites' mechanical behavior. All the lattices contained two unit cells in each direction, and the bulk dimension was 38 mm × 38 mm × 38 mm with a similar volume of about 11.2 cm^3 to ensure a fair comparison.

Foamed cement was selected as the matrix due to its wide tunable stiffness range through density control and its highly porous nature, which enables effective confinement by polymeric auxetic lattices and makes it suitable for lightweight and buoyant applications. The foamed cement paste is designed with three dry densities: 400 kg/m^3, 550 kg/m^3, and 700 kg/m^3, and the corresponding mixture proportions are listed in Table 2, where the wet density refers to the slurry density before casting and the dry density is the sample's density after 24 h drying under laboratory conditions (23 ± 2 °C and relative humidity 40 ± 10 %). To ensure a uniform distribution of the foam, a separate mixing procedure was utilized. The cement powder was first mixed with water for 2 min. Meanwhile, the foam was prepared by mixing the foaming agent with water, where the dosage of the foaming agent was determined according to the target density, and the required amount of water could be calculated based on the mixing ratio of 0.03 with respect to the foaming agent. Afterwards, the foam was mixed with the cement paste for another 2 min until no foam could be observed on the top of the surface. The foamed cement mixture was then cast into styrofoam molds where the lattice reinforcements have been previously glued. The molds were sealed with plastic foils for 3 days until demolding, and then the samples were placed in a curing room with a temperature of 20 ± 2 °C and relative humidity of 96 ± 2 %. The preparation process of the foamed cementitious composites is shown in Fig. 2. Foamed cement samples without reinforcement were also prepared for comparison. All the samples were cut into cubic shape with a size of 40 mm × 40 mm × 40 mm. The detailed information and naming convention are summarized in Table 3.

2.3. Static and cyclic compression test

Static uniaxial compression tests were conducted on 3D-printed lattices, plain foamed cement matrix, and auxetic foamed cementitious composites, respectively. The tests were performed using an UNITRONIC universal loading stage at a constant loading rate of 0.01 mm/s. To minimize boundary friction, lubricated foils were placed at the interfaces between the loading plates and the samples. Load and displacement data were recorded by the machine's loading cell and a linear variable differential transformer (LVDT), respectively. The static loading process continued until a total displacement of 18 mm was

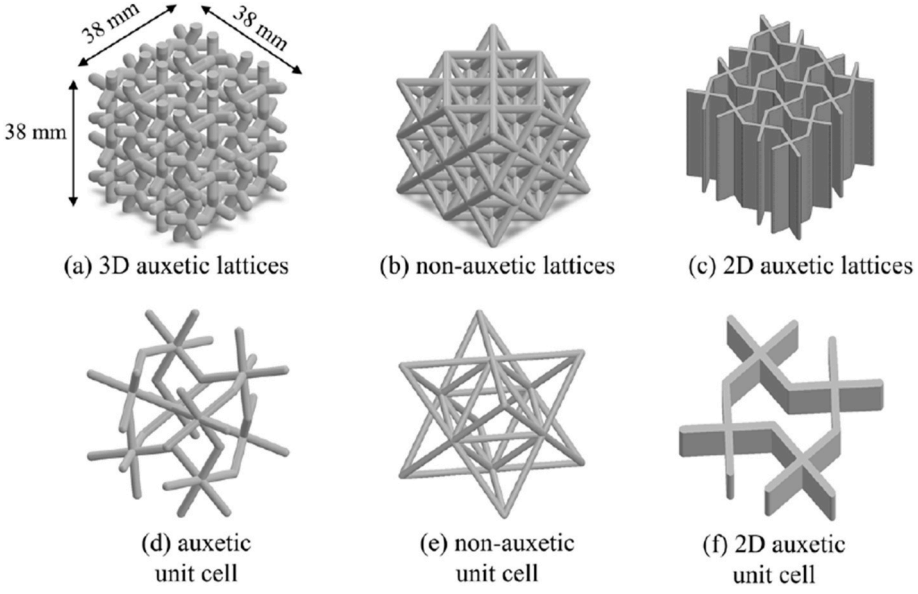

Fig. 1. Geometry designs of 3D-printed lattice structures and corresponded unit cell where smaller rib thickness was used for clear visualization purpose.

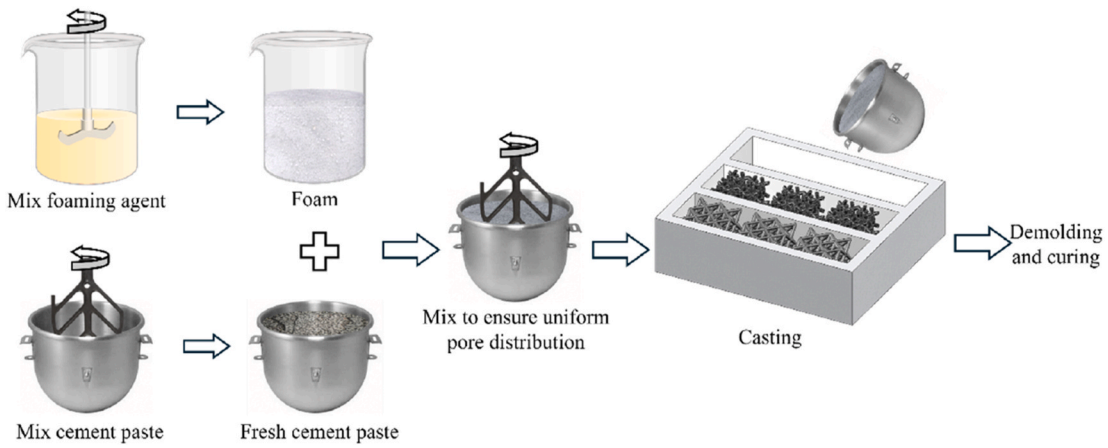

Fig. 2. Preparation procedure of the auxetic foamed cementitious composites.

Table 3
Mixture proportions of foamed cementitious matrix.

Name	Reinforcement type	Target matrix density (kg/m^3)	Measured matrix density (kg/m^3)	Measured composite density (kg/m^3)
AFCC-3D-400	3D auxetic lattice	400	418.8	584.4
AFCC-3D-550	3D auxetic lattice	550	557.3	668.0
AFCC-3D-700	3D auxetic lattice	700	701.0	723.4
AFCC-2D-550	2D auxetic lattice	550	557.3	671.9
NFCC-550	Non-auxetic lattice	550	557.3	677.3
FCP-450	–	400	418.8	–
FCP-550	–	550	557.3	–
FCP-700	–	700	701.0	–

reached, at which point the samples had fully compressed into densification.

Cyclic compression tests on the foamed cementitious composites were performed on the UTM-25 under load control mode. As illustrated in Fig. 3, two loading schemes were selected based on the results from monotonic static loading. The low load level scheme is designed to keep samples in elastic stage without inducing major cracking, reflecting the normal service conditions. The high load level scheme is designed to reach beyond the peak strength of the plain matrix, which can better refelct the lattice reinforcement effect. In the low load level scheme, a sine wave load with an amplitude of 1 kN (equivalent to 0.625 MPa, calculated based on the cross-sectional area), a mean load of 0.5 kN, and a frequency of 1 Hz was applied. In the high load level loading scheme, the amplitude was increased to 2 kN (equivalent to 1.25 MPa), and mean value was 1 kN, while the frequency remained at 1 Hz, consistent with the first scheme. Prior to cyclic loading, the samples were pre-compressed to the mean load at a rate of 0.01 mm/s. The cyclic load was applied for 1000 s, corresponding to 1000 cycles in total. Load and displacement data were recorded using the machine's loading cell and LVDT.

2.4. Digital characterization

During the static compression tests on foamed cementitious composites, black speckle patterns were applied over a white background on the specimens to facilitate digital image correlation (DIC). High-resolution images (6240 × 4160 pixels) were captured at 5-s intervals. It should be noted that two-dimensional DIC was employed, and thus out-of-plane deformations may introduce inaccuracies in the quantitative results. Nevertheless, this approach remains appropriate for qualitative assessments, such as surface crack observation.

In addition, samples after low load level cyclic test were examined using CoreTOM X-ray computer tomography (CT) system. The micro-CT scanner was operated with a voltage of 160 kV and a target power of about 25 W. The detector recorded 4283 projection images at an

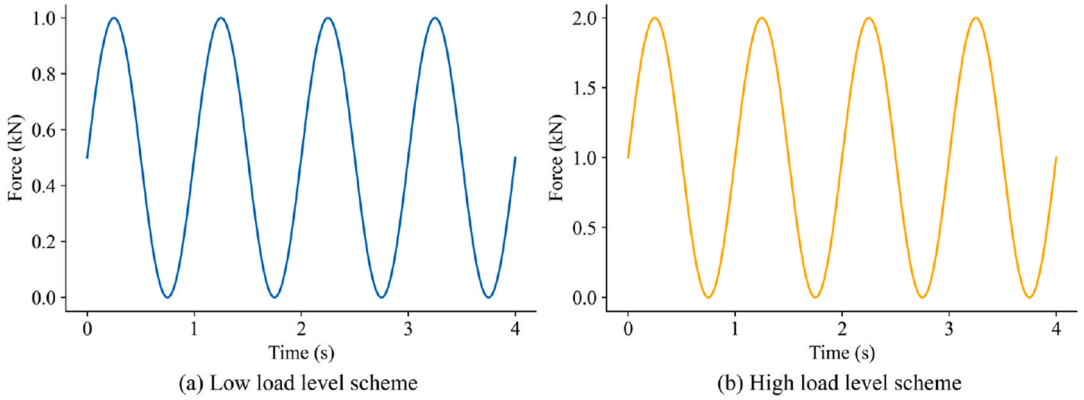

Fig. 3. Cyclic loading scheme: (a) low-load level scheme and (b) high-load level scheme.

exposure time of 190 ms each. Data were acquired at a binned pixel size of 0.15 mm, yielding images with a resolution of 2856 × 2856 pixels. The reconstructed images were then visualized using Dragonfly 3D to examine the interfacial damage between the lattice reinforcement and the foamed cement matrix.

3. Static compression: deformation behavior and load response

3.1. Mechanical properties of lattice structures

The load-displacement curves, deformation patterns, and Poisson's ratios for the 3D-printed lattice structures are shown in Fig. 4. For the 3D auxetic lattices, a load plateau is observed between 2.5 mm and 5.0 mm, corresponding to the negative Poisson's ratio region shown in Fig. 4(d). This indicates that joint buckling, which causes the load plateau, is directly responsible for the auxetic behavior. As the joints come into contact with one another, marked by the load increase from 5.0 mm, the Poisson's ratio gradually shifts into positive values, signifying the completion of the auxetic behavior. After that, the lattices are fully compacted at the end of the test, signified by a steep increase in the load. The 2D auxetic lattices exhibited the lowest stiffness and loading capacity, but the most negative Poisson's ratios. This can be attributed the smaller strut thickness (1.2 mm) compared to the other 3D structures (around 3.1 mm) to maintain the same total volume. Moreover, the in-plane design also allows for greater deformation capacity, meaning that joints come into contact at a larger displacement level. As a result, the 2D auxetic lattices exhibit a more negative Poisson's ratio and lower stiffness.

The non-auxetic lattice exhibits around 19 % higher initial stiffness and 74 % greater peak loading capacity compared to 3D auxetic lattice. This is mainly because the non-auxetic octet lattice deforms mainly through struts axial compression at the initial stage, whereas the auxetic lattice experiences joint rotation and buckling. Consequently, in design scenarios where the critical requirement is high stiffness or maximum load before damage initiation, the non-auxetic octet lattice could offer better performance. After reaching the first peak load at approximately 3.0 mm displacement, the load-displacement curves of non-auxetic octet lattices fluctuate. These fluctuations are primarily caused by sequential strut buckling layer by layer. Different from the auxetic lattices, negative stiffness can be observed in the load-decreasing regions, which is mainly attributed to strut buckling failure, while the loading capacity would start increasing again once internal joint contact occurs. This behavior repeats during the buckling of subsequent layers. As shown in Fig. 4(d), the Poisson's ratio remains positive and increases throughout compression. Unlike in 3D auxetic lattices, the load capacity does not exhibit an exponential increase, suggesting that complete densification is not reached until a 20 mm displacement. This outcome can be explained by the lateral expansion, which delays the onset of densification.

Recent literatures have highlighted that the auxetic behavior also depends on the directional response under different loading directions [53–55]. Fig. 5 compares the Poisson's ratios between 3D auxetic lattices and 2D auxetic lattices on different principal axes, where axes 1 is the loading direction. It can be noticed that the 3D auxetic lattice exhibits negative Poisson's ratios in both principal directions under compression, showing a full and multidirectional auxetic behavior before densification. In contrast, the 2D auxetic lattice shows negative in-plane Poisson's ratio, but a near-zero and even slightly positive on the

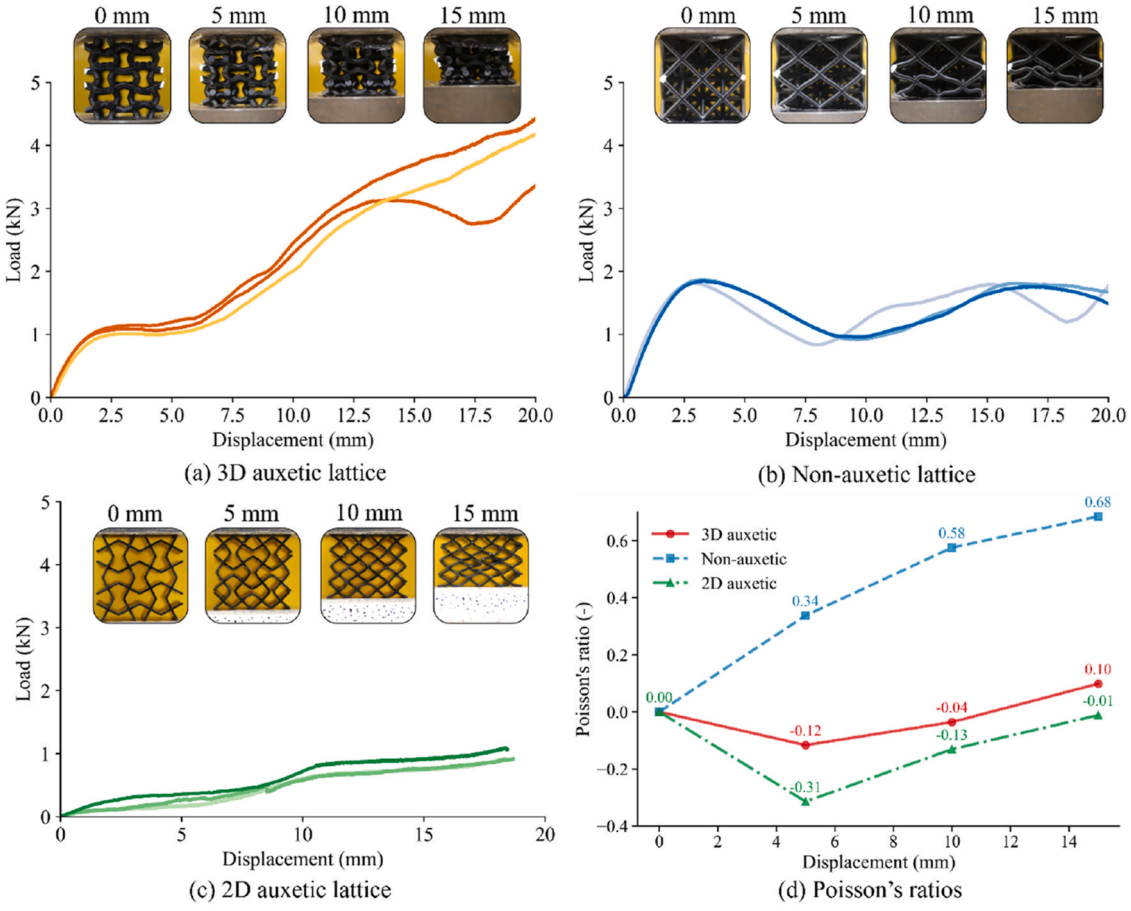

Fig. 4. Load-displacement curves, deformation patterns, and Poisson's ratio evolution for different lattice structures: (a) load-displacement curves for 3D auxetic lattices; (b) load-displacement curves for non-auxetic lattices; (c) load-displacement curves for 2D auxetic lattices; (d) Poisson's ratios.

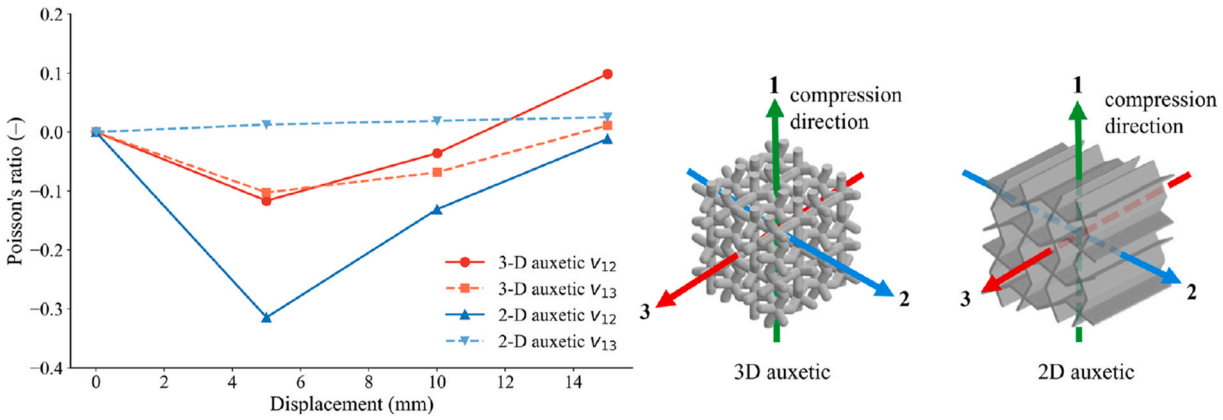

Fig. 5. Poisson's ratios of 3D auxetic lattices and 2D auxetic lattice on different directions.

out-of-plane direction can be also observed, demonstrating a partial auxetic behavior. This partial auxeticity in the 2D design indicates a limited confinement on principal axes 3 and could contribute to mechanical behaviors of the foamed cementitious composites.

3.2. Mechanical properties of auxetic foamed cementitious composites

The load-displacement curves and specific energy absorption (defined as the amount of energy absorbed per unit mass, J/g) for foamed cementitious composites reinforced with different lattice structures are shown in Fig. 6, where AFCC-3D stands for foamed cementitious composites with 3D auxetic reinforcement, and AFCC-2D represents the one reinforced with 2D auxetic lattice, and NFCC stands for foamed cementitious composites with non-auxetic lattice, and FCP represents the reference foamed cement paste samples without any reinforcement. The number 550 is the dry density of the matrix in kg/m^3.

As shown in Fig. 6(a), both 3D auxetic and non-auxetic lattices can improve the load bearing capacity and the ductility of foamed cementitious composites compared to the reference (FCP-550). The reference sample reached a peak load of 1.7 kN at 0.6 mm. For 3D auxetic and non-auxetic lattice reinforced samples, the peak load is defined at the yield-like transition point where the slope decreases, indicating a shift from initial stiff behavior to a softer response. Although the peak loads for AFCC-3D-550 and NFCC-550 samples were nearly the same at a displacement of 1.5 mm, the corresponding load capacity at 1.5 mm for the 3D auxetic lattice reinforcement was 0.9 kN, which is lower than the 1.3 kN observed for the non-auxetic lattice in Fig. 4. This finding indicates that lateral contraction from the auxetic behavior helps confine the matrix, thereby enhancing the composite's overall loading capacity, even though the auxetic lattice itself has a lower standalone load-bearing capacity compared to its non-auxetic counterpart. Afterwards, the 3D auxetic lattice reinforced foamed cementitious composites entered the densification stage from approximately 5 mm (densification stage is identified as the load starts to increase steeply after a plateau, and more detailed definition can be found in literature [48]), whereas the non-auxetic counterparts maintained a load plateau until around 10 mm. This behavior aligns with the standalone mechanical response of the lattices, where the lateral contraction induced by auxetic behavior leads to earlier densification in both the lattice and the composite, while the expansion tendency of non-auxetic lattices extends the plateau phase, delaying densification.

For composites reinforced with 2D auxetic lattices, the peak load was lower than that of the matrix, despite a hardening stage observed due to the gradual compaction of the embedded 2D auxetic lattice. This reduced load bearing capacity is partly contributed to the lower load bearing capacity of the 2D auxetic lattice itself, and is also due to the lack of out-of-plane confinement. In contrast, 3D auxetic lattices can provide negative Poisson's ratios in both in-plane and out-of-plane directions, thereby offering superior structural reinforcement effect on the matrix. Furthermore, the designed 2D auxetic lattices have a 70 % larger surface area compared to their 3D counterparts, making them more susceptible to interfacial debonding, which may further limit the overall load-bearing capacity of the composite.

The specific energy absorption capacities in Fig. 6(b) showed that the 3D auxetic lattice reinforced foamed cementitious composites exhibit the highest energy absorption capacity, followed by the non-auxetic reinforced ones, 2D auxetics reinforced ones. The superior energy absorption of AFCC-3D-550 is attributed to the auxetic lattice's negative Poisson's ratios and earlier transition into densification, which provides

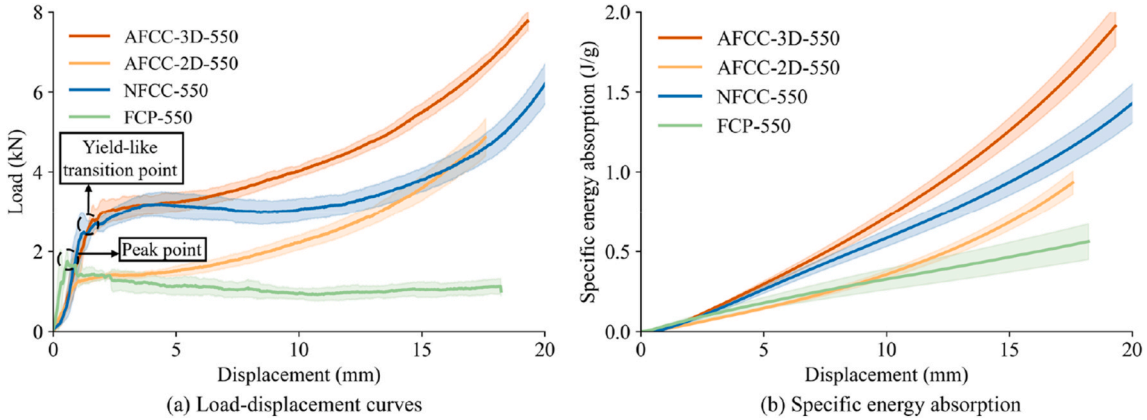

Fig. 6. Load-displacement and specific energy absorption curves of foamed cementitious composites reinforced with different lattice structures.

enhanced confinement and load distribution throughout the matrix. As for composites reinforced with 2D auxetic lattices, the specific energy absorption remained higher than that of the foamed cement matrix at higher loading levels due to the auxetic behavior induced in-plane contraction. This suggests that, although 2D auxetic lattices contribute to improved ductility and energy absorption efficiency, their performance could be further optimized by incorporating out-of-plane reinforcement mechanisms.

The DIC results are shown in Fig. 7. Although only damage or crack distributions over the exterior surface can be monitored, the DIC results can still exhibit distinctly different patterns and crack progression behaviors. In the 3D auxetic composite (AFCC-3D-550) the first crack appears at about 1.0 mm displacement, which is roughly 0.3 mm later than that in the plain matrix. Subsequently, a few smaller cracks start to form along the free edges, where the lattice offers the least confinement. But the cracks still remain diffuse, indicating a distributed damage distribution. For 2D auxetic reinforced composites (AFCC-2D-550), cracks initiated at a similar displacement level, but cracks propagate horizontally across the mid-height region that most lacks out-of-plane confinement, producing more concentrated crack distribution patterns. In terms of NFCC-550 sample, cracks start to appear at the specimen corners, and then propagate on diagonal paths toward the central area, following the octet lattice strut orientation. Afterwards, the diagonal shaped cracks gradually merge to form an X-shaped shear band, which is caused by the positive Poisson's ratio expansion of non-auxetic lattice. By contrast, a single vertical crack forms and propagates rapidly in the plain foamed cement paste (FCP-550), exhibiting a sudden transition between 0.5 mm and 0.7 mm displacement, which is also marked as the peak load of FCP-550 in the load-displacement curves. Together these observations further confirm that absence of lattice reinforcement could result in reduced ductility and a limited ability to redistribute stress.

The failure states at the end of the test have been shown in Fig. 8, where the red dashed line marks the original dimension of the sample. In the composite reinforced with the 3D auxetic lattice, the unconfined exterior cover crumbled, but the lattice forced the remaining core to contract laterally, making the final width smaller than original cross-section, showing auxetic behaviors at the composite level. This suggests that the auxetic lattice can effectively confine the lateral expansion and contribute to the densification and hardening stage. In the specimen with 2D auxetic, the core contracts as well, but the absence of confinement in the third (out-of-plane) direction causes severe out-of-plane fragmentation. The non-auxetic lattice composite behaves oppositely: the sample expands laterally which is in line with the lattice's positive Poisson ratio. This could also explain the longer plateau before densification seen in the load–displacement curve. Contrary to the diffuse crack distributions for samples with lattice reinforcement, the reference plain matrix was split by a major crack at the end of the test, and the sample size was also slightly larger than the original one.

3.3. Influence of matrix density on AFCC

To focus on how matrix density and curing age influences the contribution of auxetic reinforcement, this and next sections will compare the 3D auxetic foamed cementitious composite with its plain foamed-cement paste. Fig. 9 compares the mechanical properties of plain foamed cement samples and 3D auxetic reinforced composite samples with varying matrix densities (400 kg/m^3, 550 kg/m^3, and 700 kg/m^3). As indicated in Fig. 9(a), the peak load and stiffness of plain foamed cement samples increase with higher matrix density due to

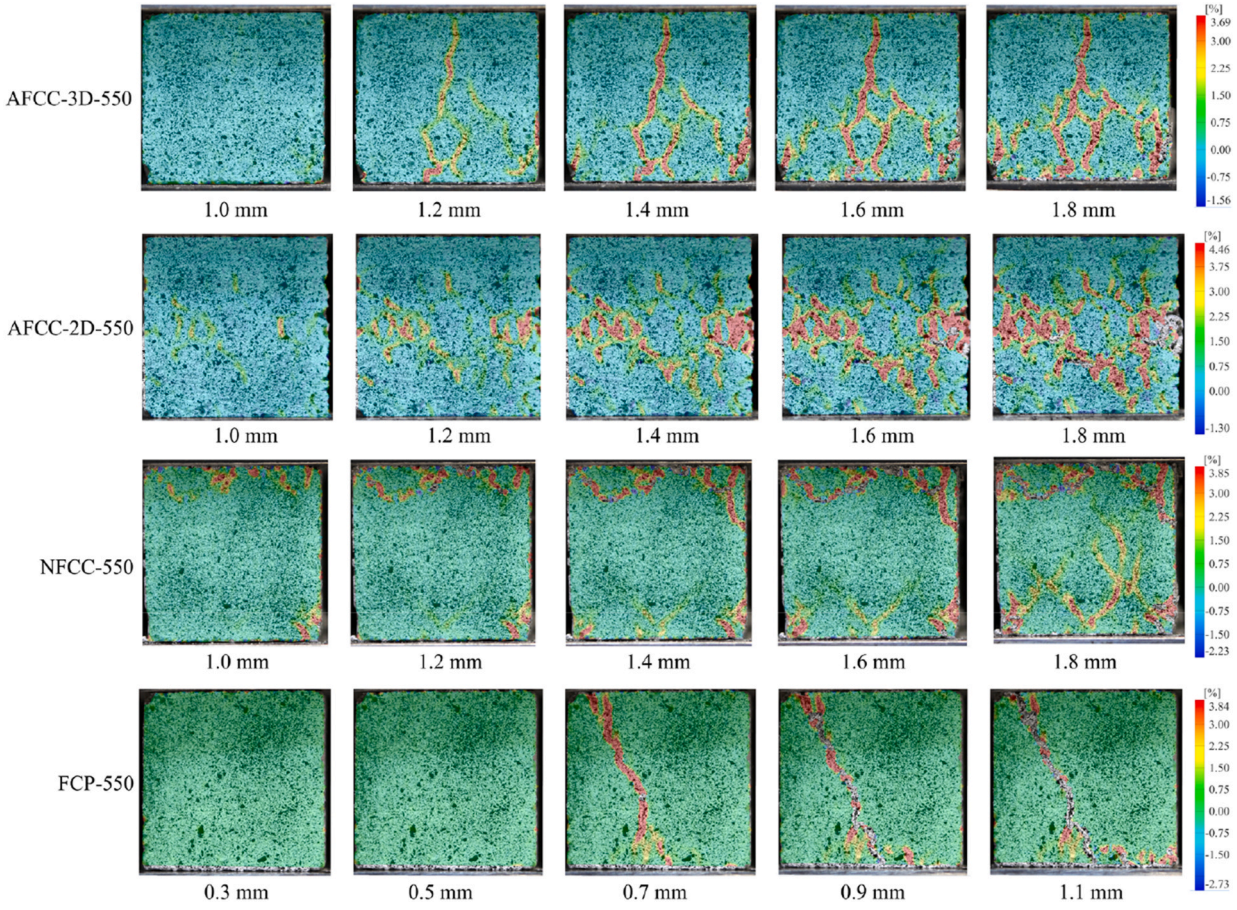

Fig. 7. Digital image correlation results for foamed cementitious composites and foamed cement with a matrix density of 550 kg/m^3.

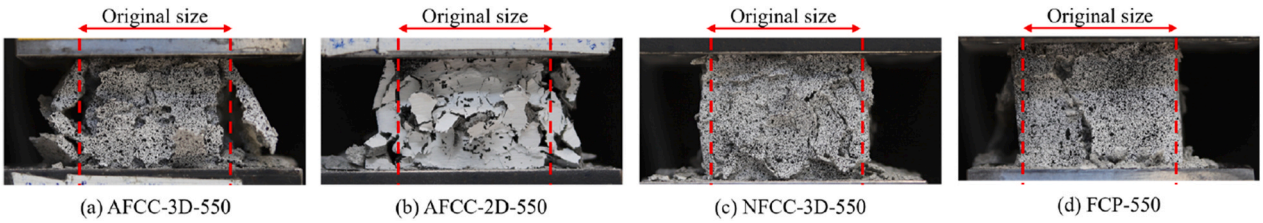

Fig. 8. Failure states at the end of the test with a compressive displacement of 18 mm.

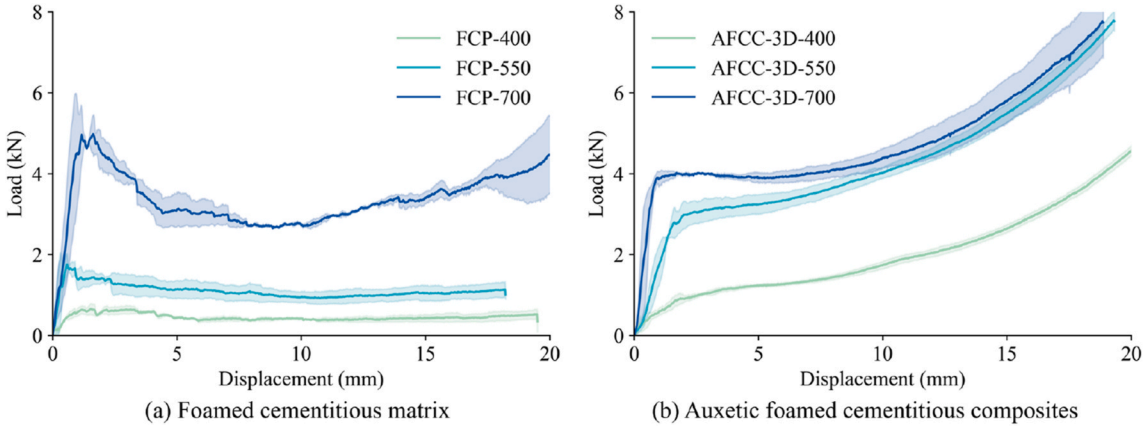

Fig. 9. Load-displacement curves of foamed cementitious matrix and composites with different matrix densities.

improved material density. FCP-700 reaches the highest peak load (around 5 kN) but also exhibits pronounced load capacity drop due to brittle fracture behavior of cement matrix. On the other hand, foamed cementitious matrices with lower densities (i.e., FCP-550 and FCP-400) show gradual load plateaus, indicating a foam-like progressive crushing behavior.

In Fig. 9(b), for composites with a matrix density of 400 and 550 kg/m^3, the AFCC-3D samples exhibit significantly enhanced strength and ductility compared to the unreinforced matrix. AFCC-3D-400 demonstrates a more gradual and sustained load increase than the plain matrix, indicating that auxetic lattice reinforcement aids in stress redistribution following matrix damage. In contrast, AFCC-3D-700 exhibits a lower peak load than its corresponding matrix. This is primarily because, at a density of 700 kg/m^3, the strength and stiffness of the matrix surpass those of the auxetic lattice, making the embedded lattice the weaker component in the composite system, thereby reducing the overall peak load. However, AFCC-3D-700 reaches the densification stage at around 7 mm (indicated by the load start to increase exponentially), while the matrix started to densify from around 15 mm. This suggests that, as the matrix undergoes damage, the auxetic lattice gradually becomes the stiffer component, which enables the auxetic reinforcement to continue confining the matrix and maintaining composite integrity despite matrix degradation.

Additionally, it can be seen that, as the matrix density increases, the auxetic foamed cementitious composites reach the load plateau at lower displacements. Conversely, for low-stiffness matrix (e.g., AFCC-3D-400), the auxetic lattice needs more deformation to compress the matrix before reaching a balanced state, making the load plateau stage less obvious. Besides, the highly porous nature makes the matrix unable to resist joint buckling of the auxetic lattice, making it more susceptible to local damage around lattice joints. This localized failure could then propagate into macro cracks under high strain level, thereby compromising the overall mechanical performance. These findings emphasize the importance of optimizing the stiffness balance between the auxetic lattice and the matrix to maximize both the strength and the energy dissipation in foamed cementitious composites.

The specific energy absorption capacities up to 16 mm displacement are shown in Fig. 10. For matrix density of 400 kg/m^3, the reinforcement of auxetic lattice reinforcement can improve the specific energy absorption of 2.57 times, while the auxetic lattice reinforced cementitious composites with a matrix density of 550 kg/m^3 is 2.8 times of the reference plain matrix. However, when the matrix density further increased to 700 kg/m^3, the specific energy absorption ratio between auxetic reinforced composites and reference matrix was only 1.3. This indicates that the effectiveness of auxetic lattice reinforcement in enhancing energy absorption is more pronounced in lower-density matrices but becomes less significant as matrix stiffness increases. At 400 kg/m^3 and 550 kg/m^3, the matrix is relatively porous and soft, allowing the auxetic lattice to play a dominant role in constraining lateral expansion, promoting gradual densification and improved energy absorption. However, at 700 kg/m^3, the stiffer and stronger matrix begins to dominate the mechanical response, reducing the relative contribution of the auxetic lattice. In this case, because the auxetic lattice is inherently more deformable than the high-density matrix, it may

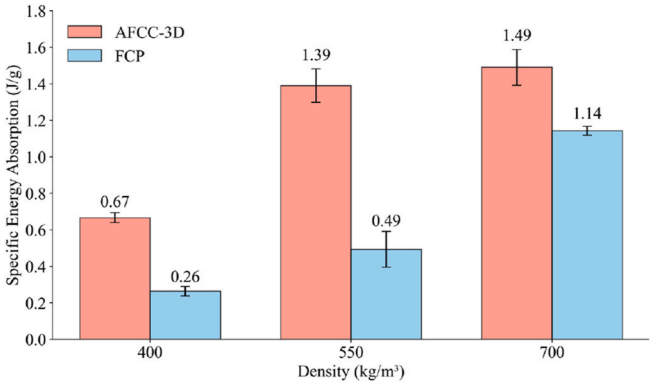

Fig. 10. Specific energy absorption capacities up to 16 mm displacement of foamed cementitious matrix and composites with different matrix densities.

act as a weaker component within the composite, limiting the further improvement on load resistance and energy absorption capacity.

3.4. Influence of curing ages on AFCC

Fig. 11 presents the load-displacement behavior of foamed cement paste (FCP) and 3D auxetic foamed cementitious composites (AFCC-3D) at 14 and 28 days of curing, with a matrix density of 550 kg/m^3. For the reference foamed cement matrix, the 28-day samples exhibit a moderate increase in peak load and stiffness compared to their 14-day counterparts. However, this improvement remains relatively limited due to the inherent porosity of the matrix. The load plateau phase remains similar between FCP-14days and FCP-28days, suggesting that matrix compaction primarily governs the post-peak mechanical response rather than age-related strength improvements.

In contrast, the AFCC-3D samples show an obvious increase in strength between 14 and 28 days, highlighting the effectiveness of auxetic lattice reinforcement in enhancing the mechanical performance as the matrix gains strength. The AFCC-28days sample exhibits a significantly higher load capacity compared to AFCC-14days, indicating that, as the cementitious matrix strengthens, the auxetic lattice can provide better constraint effectiveness and stress redistribution on the matrix. It suggests that because of the more effective confinement from the auxetic lattice, the matrix can withstand higher load without showing premature failure. However, AFCC-28days displays a lower initial stiffness than FCM-28days, whereas AFCC-14days exhibits an initial stiffness similar to that of FCM-14days. This is because, at earlier curing stages, the weaker matrix has similar stiffness compared to the deformable auxetic lattice, so the inclusion of polymeric lattice does not significantly alter stiffness. As the matrix strengthens over 28 days, the more deformable auxetic lattice reduces the overall stiffness of the composite.

4. Cyclic compression: load response and internal damage

4.1. Responses at low load level cyclic test

In the low-load cyclic test, a sine wave load with an amplitude of 1 kN and a mean value of 0.5 kN was applied. The samples with a matrix density of 550 kg/m^3 after 28-day curing were used in the cyclic test. Under a load level of 1 kN, the static loading test in Section 3 shows that both foamed cementitious composites reinforced with 3D auxetic lattices and reference foamed cement paste remained within the linear elastic region. However, the 2D auxetic lattice-reinforced composites were close to the transition point into the plateau stage.

The cyclic load–displacement responses during 1000 cycles are shown in Fig. 12, where the horizontal axes were kept as the same scale for clearer comparison. For AFCC-3D-550, NFCC-550 and FCP-550 in Fig. 12(a)–(c), the load–displacement loops from cycles 0 through 1000 remain relatively narrow and closely grouped. For instance, AFCC-3D-550 shows displacement amplitudes below approximately 0.30 mm, increasing from the initial loop (purple) to the final loop (yellow). Similarly, the NFCC-550 exhibits low displacements, although the curves extend horizontally to around 0.60 mm, which is slightly larger than the auxetic counterparts. The plain foamed cement paste reference stays in an even smaller displacement range, which is less than 0.12 mm, indicating a higher stiffness which is consistence with observations in monotonic static loading. Compared to the foamed cement paste reference, the relatively larger displacement range of lattice reinforced foamed cementitious composites is attributed by the interaction slip between lattice structure and matrix, which will be observed in the CT images. Nevertheless, these observations suggest that the composites reinforced with both 3D auxetic and non-auxetic lattices, as well as the plain foam cement paste could remain in a relatively stable state without any obvious damage or degradations under low load level over 1000 cycles.

In contrast, the foamed cementitious composites with 2D auxetic reinforcement exhibits much larger displacements (on the order from 0.5 mm to over 2.0 mm), as shown in Fig. 12(d). While the overall load remains the same at 1 kN, each successive loop shifts toward higher displacements, implying a more pronounced deformation. This suggests that the sample undergoes incremental compaction to compensate the stiffness loss due to matrix damage. This behavior is consistent with the composite being on transition point into the plateau region as seen in the static monotonic test. In addition, the lack of confinement on the out-of-

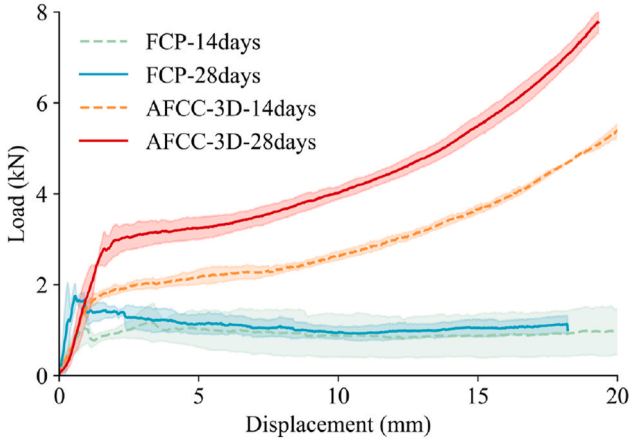

Fig. 11. Load-displacement curves of foamed cementitious matrix and composites with different curing ages.

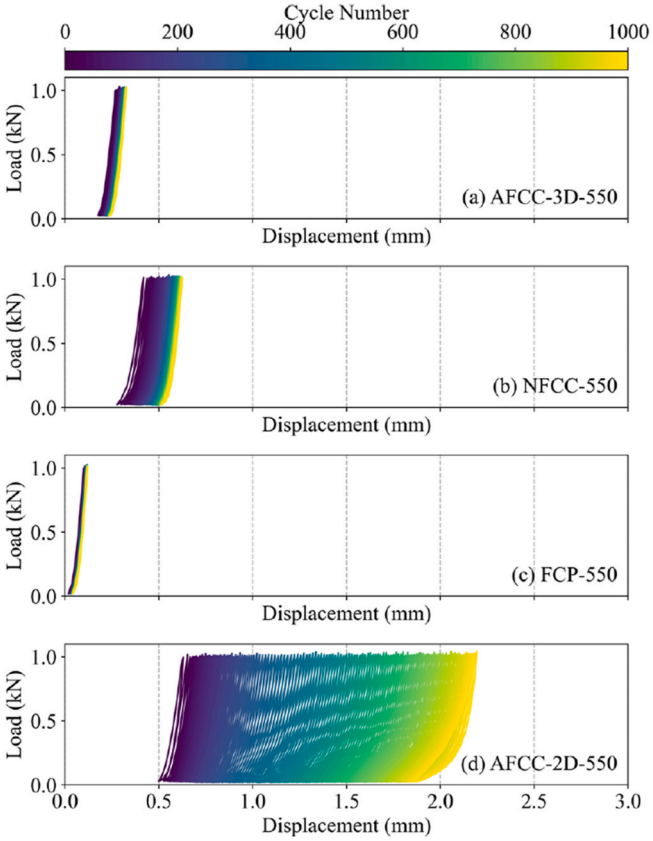

Fig. 12. Cyclic load-displacement curves under low load level loading: (a) AFCC-3D-550 (foamed cement composite with 3D auxetic lattice), (b) NFCC-550 (foamed cement composite with non-auxetic lattice), (c) FCP-550 (foamed cement paste), and (d) AFCC-2D-550 (foamed cement composite with 2D auxetic lattice).

plane direction for the 2D auxetic lattice may also contribute the reduced stiffness during cyclic loading. Although larger hysteretic displacement is beneficial to higher energy the dissipation capacity for 2D auxetic-reinforced foamed cementitious composites under cyclic loading, the faster stiffness degradation and accumulation of internal damage caused by larger displacement should also be kept in mind.

After 1000 low load level cycles, the AFCC-3D-550, NFCC-550, and AFCC-2D-550 samples were scanned by XCT. Fig. 13 shows reconstructed images of 3D auxetic reinforced composite sample. Because cracks and pores appear at similar gray levels, it is challenging to distinguish them solely by grayscale segmentation; therefore, only representative slices from the left, central, and right unit cells were extracted and analyzed. The dark region highlighted with the red dashed box represents the low-density damaged area in foamed cement paste, while the orange areas represent the embedded lattice reinforcement.

It can be observed from the figure that, in side slices, the damaged area is mainly concentrated around the lattice joints or edges. This occurs because the auxetic lattice relies on joint buckling to achieve its negative Poisson's ratio, and the joints undergo higher deformation than the rest of the lattice. Consequently, the surrounding matrix at these joints is more prone to damage from repeated cyclic loading. On the contrary, significantly less damage appears in the middle slices. This can be explained by the matrix in the middle slice being primarily in a confined state: horizontal struts compress the matrix in multiple directions, reducing the damage degree. Furthermore, the central unit cell shows less damage in its middle slice compared to the left and right unit cells. Although damage still occurs in these central slices, it is generally located near the outer boundaries rather than the core. This suggests that the interior region of the lattice unit cell experiences a stronger confinement effect, leading to reduced damage.

The damage observed at the lattice–matrix interface also provides insight into the larger displacement amplitude in reinforced samples compared to the foamed cement paste alone. Under cyclic loading, the auxetic lattice reinforcement needs first to deform through the damaged interface region before it can effectively engage with the surrounding matrix. As a result, a greater displacement amplitude is required to attain the target load of 1 kN. This suggests that, for soft matrices such as foamed cement paste, the mechanical properties perpendicular to the interface could influence the overall performance. Due to the brittle and porous nature of foamed cement matrix, the interfacial cement paste is more likely to fracture first under loading, particularly when the reinforcement has a higher stiffness. Following their fracture, the reinforcement compacts the matrix until a balance is reached, where the matrix can oppose the movement of the reinforcement and the reinforcement itself can provide confinement to the matrix.

Fig. 14 depicts the reconstructed volume of the non-auxetic lattice reinforced foamed cementitious composite (NFCC-550), along with representative planar slices extracted from different positions. The orange components correspond to the non-auxetic lattice reinforcement, while red dashed ellipses highlight dark areas of damaged low-density regions in the slices. Across all unit cells, damage tends to concentrate near the lattice nodes and is oriented along the adjacent diagonal struts, suggesting that shear stresses between the matrix and the diagonal reinforcement members is the major reason for the damage. This inside damaged pattern is also similar with the surface damaged pattern observed in DIC. Moreover, unlike auxetic lattices, which contract laterally under compression and thereby providing a more uniform confinement to the matrix, non-auxetic lattices expand laterally when compressed. This lateral expansion induces localized shear force at the interface since the stiffer reinforcement attempts to move outward against the surrounding cement paste. Consequently, the brittle and porous cement matrix close to the diagonal rods would fracture or detach, leading to a more extensive damaged region compared to the auxetic counterpart. Such interfacial shearing is also reflected in the larger displacement ranges for NFCC-550 sample during cyclic loading, as the reinforcement struts must slip relative to the matrix before effective load transfer occurs. Therefore, the overall response in NFCC-550 is governed by an interplay between diagonal strut expansion, matrix shear failure, and the interaction of the non-auxetic lattice with the surrounding foamed cement paste.

The damage distribution pattern for 2D-auxetic reinforced cementitious composites (AFCC-2D-550) are shown in Fig. 15. The 2D auxetic lattice primarily provides in-plane confinement (i.e., within the vertical slice), causing cracks to propagate in the direction which lacks confinement. As indicated by the red dashed lines in the horizontal slice, multiple longitudinal cracks develop through the thickness of the

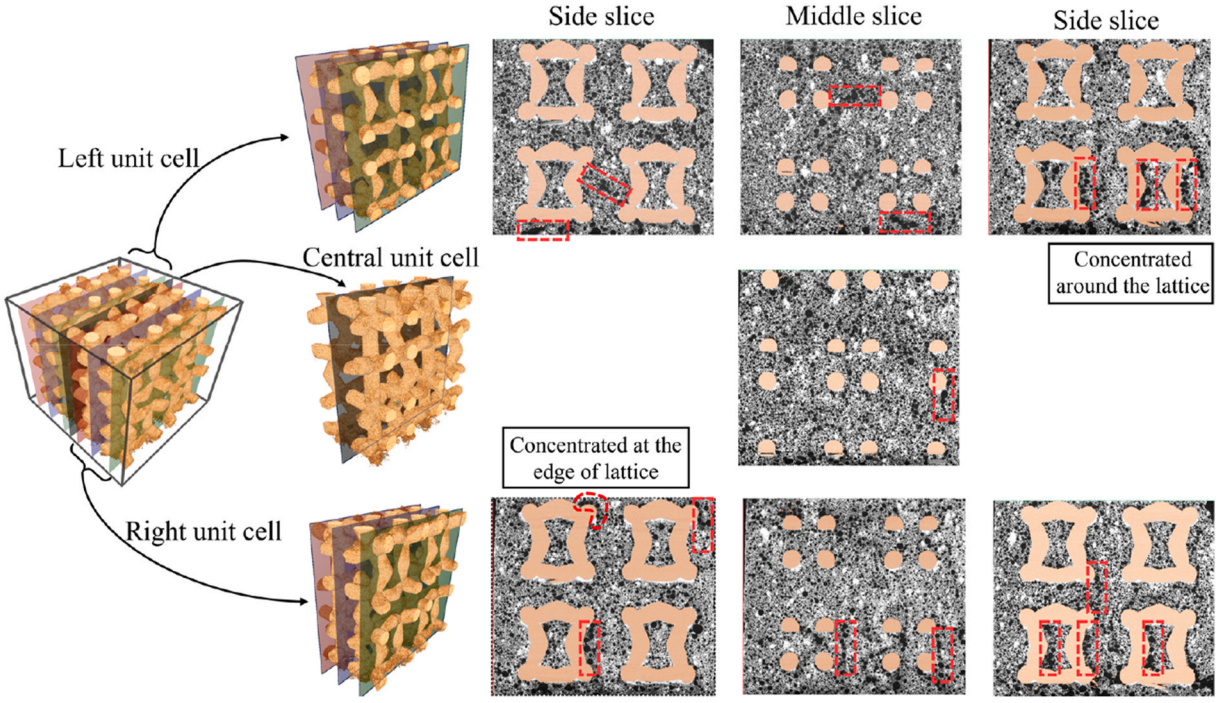

Fig. 13. Reconstructed CT images for foamed cementitious composites with auxetic reinforcement.

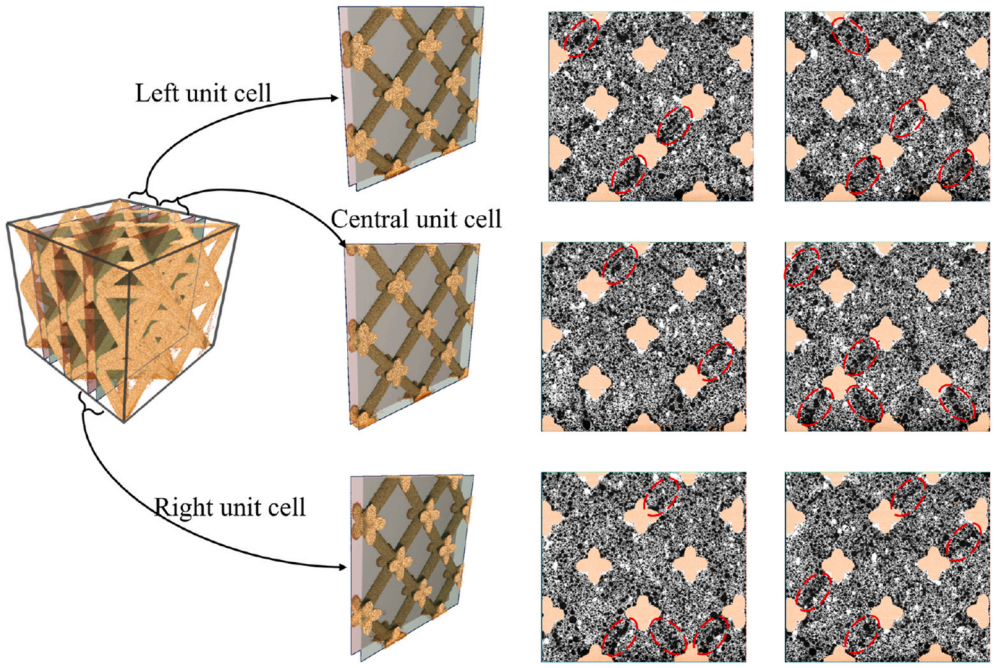

Fig. 14. Reconstructed CT images for foamed cementitious composites with non-auxetic reinforcement.

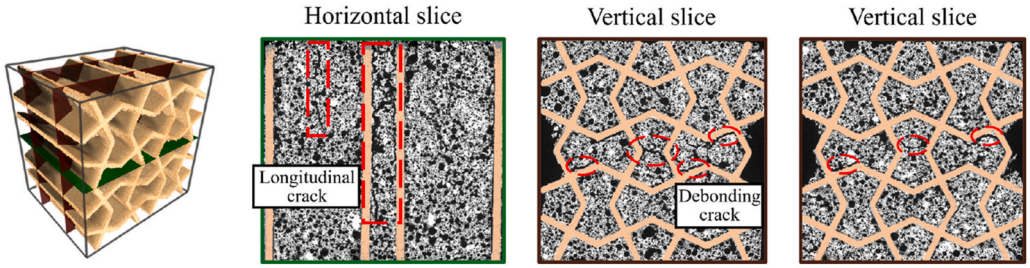

Fig. 15. Reconstructed CT images for 2D-auxetic lattice reinforced foamed cementitious composites.

sample, suggesting that the partial confinement in the 2D auxetic lattice is insufficient to effectively prevent such fracture paths. Meanwhile, debonding cracks appear along the interface between the polymeric lattice and the surrounding foamed cement matrix. This phenomenon arises from two principal factors: first, the 2D lattice's relatively low stiffness makes it more prone to deformation, and second, the substantial stiffness difference between the polymeric lattice and the cementitious matrix also contributes the stress concentrations along the interface. Consequently, localized debonding is more likely to occur, undermining the overall effectiveness of the 2D auxetic reinforcement in restraining crack development.

4.2. Responses at high load level

Under a higher loading condition (2.0 kN amplitude and 1.0 kN mean load), most specimens experienced abrupt failure, whereas the 3D auxetic foamed cementitious composite (AFCC-3D-550) showed a ductile-like damage pattern instead of sudden failure. Fig. 16 compares the maximum displacement in each cycle, while Fig. 17 displays all available cyclic load–displacement responses during the test under the same displacement scale. From the maximum displacement curves, only the AFCC-3D-550 sample continued to sustain cyclic loading beyond 500 cycles, ultimately reaching 700 cycles without a sudden failure. The gradually increased maximum displacement per loop indicates a progressive damage mechanism, wherein microcracks and local interface damage initiates from lattice joints due to the buckling tendency, while

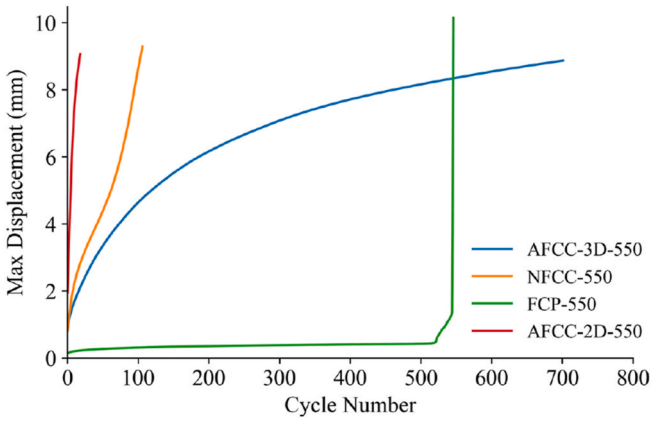

Fig. 16. Maximum displacement each cycle under high load level cyclic test.

at central of the unit cell the confinement from lattice struts can delay damage propagation through the matrix. This behavior is supported by the hysteresis loops observed in Fig. 17(a): after an initial shift toward larger displacement, the loops tend to stabilize as cycle numbers increase, which is indicated by the large portion of purple-colored loops covering most of the displacement range. This indicates that the early rise in displacement is primarily driven by localized damage near the

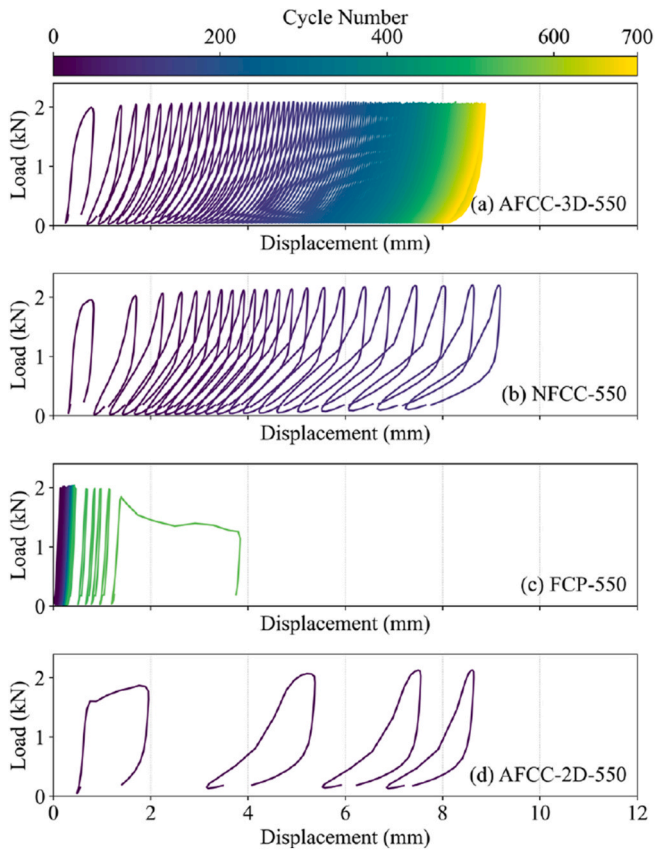

Fig. 17. Cyclic load-displacement curves under high load level cyclic loading: (a) AFCC-3D-550 (foamed cement composite with 3D auxetic lattice), (b) NFCC-550 (foamed cement composite with non-auxetic lattice), (c) FCP-550 (reference foamed cement paste), and (d) AFCC-2D-550 (foamed cement composite with 2D auxetic lattice).

lattice joints. Furthermore, the width of hysteric loop did not show significant change until the end of the test, which also indicates a stable energy absorption capacity under high-load-level cyclic conditions.

The non-auxetic foamed cementitious composite (NFCC-550) shows a rapid rise in terms of maximum displacement within the first 100 cycles, reaching a maximum displacement of around 9 mm at failure, as shown in Fig. 16. This rapid deformation mainly results from the lateral expansion of non-auxetic lattice, which provides limited structural confinement and vertical support under high-load-level cyclic compression. In Fig. 17(b), the cyclic loops of the NFCC-550 sample are all within purplish color, indicating that they are limited to the first 100 cycles. During this stage, the loops shift quickly toward larger displacements, suggesting that internal damage progresses faster compared to the 3D auxetic system. This accelerated deterioration comes from the lateral expansion and strut buckling of non-auxetic lattice, which undermine the composite integrity and eventually lead to structural failure.

In contrast, the plain foamed cement paste (FCP-550) displays the lowest maximum displacement per cycle over the first 500 cycles, suggesting a rigid response. Because it lacks any plastic-based lattice structure and reinforcement–matrix slip, it requires less displacement to achieve the target load amplitude. However, once its limited ductility is exceeded, there is a sudden jump in displacement, showing a catastrophic crushing to reach the 2.0 kN amplitude. This sharp rise at around 500 cycles indicates a brittle failure, aligning well with the major cracking and fragmentation of the sample. Fig. 17(c) shows that the load-displacement loops gradually broaden during the first 400 cycles. At around 500 cycles, the displacement amplitude suddenly increases, as indicated by the sharp expansion of the loops. This also indicates the FCP sample can retain a relatively high stiffness over these initial cycles, but in the absence of reinforcement to mitigate local damage or redistribute stress, its limited ductility is eventually surpassed, resulting in an abrupt failure.

In terms of 2D auxetic foamed cementitious composite (AFCC-2D-550), Fig. 16 shows that it failed very early in the test within the first few cycles, as indicated by the rapid increase in the max displacement curve and abrupt termination at a displacement of around 9 mm reaching the protection displacement range of the machine. The lack of out-of-plane confinement in the 2D lattice induces the matrix spalling and crack propagation is responsible for the premature failure of AFCC-2D-550 samples. In addition, Fig. 17 also confirms that all the hysteric loops are located within the first few cycles as plotted in purple, and the width of each hysteric loop gradually become narrower, which also indicates the unrecoverable damage and reduced energy absorption capacity of the composite.

The ultimate failure patterns at the end of the high load cyclic test are illustrated in Fig. 18. Due to sample vibration during cyclic loading, only the final damage states recorded at the end of the tests are presented. The 3D auxetic foamed cementitious composite (AFCC-3D-550) exhibited only minor surface crumbling while retaining its overall structural integrity. The AFCC-3D-550 sample sustained the high load level cyclic compression beyond 700 without a sudden catastrophic collapse, which suggests the ductile failure mode compared to the plain foamed cement paste. In contrast, the foamed cementitious composite with 3D non-auxetic lattice endured only up to approximately 100 cycles before collapse occurred and the loading apparatus reached the maximum displacement. As shown in Fig. 18(b), the struts buckling and lateral expansion of the non-auxetic reinforcement, which induced the lack of confinement of the matrix, eventually contributed to this progressive compression and failure mode. Similarly, the plain foamed cement paste in Fig. 18(c) exhibited a brittle, explosive failure mechanism characterized by extensive cracking and fragmentation of the cement matrix, resulting in an almost complete loss of integrity. Meanwhile, as shown in Fig. 18(d), although the 2D auxetic lattice reinforced specimen retained some outline of the lattice, the sample still suffered substantial matrix spalling, and reached the displacement limit of the machine less than 100 cycles, This rapid loss of load carrying capacity, accompanied by a large displacement jump, highlights a sudden failure pattern for the 2D auxetic lattice reinforced system under high load level cyclic compression.

5. Conclusions

In this paper, the mechanical performance of 3D-printed lattice reinforcements in foamed cementitious composites under both static and cyclic loading was systematically investigated. The study encompassed three different lattice designs (3D auxetic, 2D auxetic, and non-auxetic) and varied the matrix density from 400 kg/m^3 to 700 kg/m^3. Through uniaxial compression testing, cyclic loading test, digital image correlation, and X-ray computed tomography, the reinforcing mechanisms and damage evolution in these lightweight composites. One of the most significant findings is that 3D auxetic lattice reinforced foamed cement composite not only increases peak compressive strength and extends post-peak ductility but also sustains over 700 high-load cyclic compression cycles without brittle failure. These results illustrate the application of negative Poisson's ratio architectures in improving both strength and toughness of foamed cement, highlighting the potential of architecture lattice structure to advance high-performance lightweight concretes.

1. Under high-load cyclic conditions, 3D auxetic lattice-reinforced foamed cementitious composites showed pronounced resilience, exhibiting gradual and ductile damage evolution while sustaining performance well beyond 700 cycles. In contrast, all other groups suffered abrupt or premature failures. At lower cyclic loading levels,

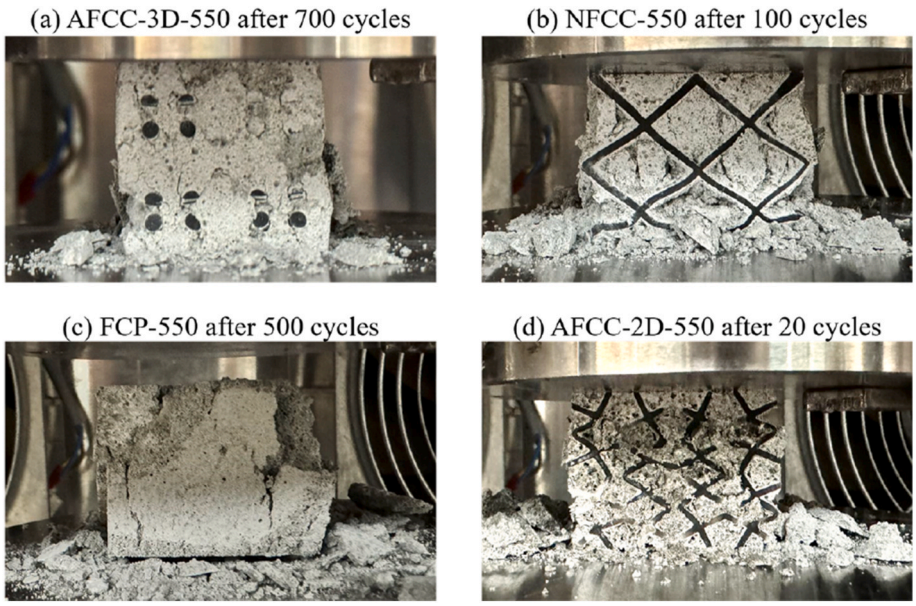

Fig. 18. Failure patterns after high load cyclic compression test.

only 2D auxetic-reinforced composites exhibited greater displacement due to accumulated out-of-plane damage, while the 3D lattice-reinforced samples remained structurally stable.

2. X-ray computed tomography revealed that, after low-load cyclic loading, the damage in composites with 3D auxetic lattice was localized near lattice joints, which was attributed to joint buckling necessary for auxetic behavior. Nonetheless, the overall matrix core remained relatively confined. In contrast, non-auxetic lattices prompted shear failure along diagonal struts, and 2D auxetic lattices exhibited more pronounced spalling due to limited out-of-plane support.
3. Negative Poisson's ratio behavior enables earlier densification by effectively confining the matrix, which is why 3D auxetic lattices showed the greatest improvements in strength, ductility, and energy absorption. Non-auxetic lattices offered moderate benefits, but these were less pronounced at higher strain levels. Meanwhile, 2D auxetic lattices, being limited to in-plane confinement, yielded lower improvements compared to the reference matrix.
4. Auxetic lattice reinforcement yielded more pronounced benefits at matrix densities between 400 kg/m^3–550 kg/m^3, where the lattice could more effectively mobilize its lateral contraction to confine the softer matrix. At higher density (700 kg/m^3), the stiffer matrix overshadowed the auxetic effect from soft polymeric lattice, resulting in reduced strength and lower energy absorption enhancement. However, as matrix degradation progressed, the lattice gradually took the dominant role in resisting load, resulting in earlier densification compared to the plain matrix.

Although the presented foamed cementitious composites with auxetic lattices showed substantial mechanical improvements while maintaining lightweight features compared to traditional foam concrete, there are still some aspects that require further investigation. First, the size effect of the composite can be further studied, and the foam stability in smaller size and lattice printability in larger size should be paid special attention. Secondly, although the influence of different lattice-matrix volume ratio can be partially reflected through varied matrix density, this impact on the mechanical properties needs to be more explicitly clarified by varying the lattice volume without compromising foam stability during casting. Finally, a systematic study of other alternative lattice architectures (e.g., simple-cubic designs with zero Poisson's ratios) and their influence of foamed cementitious composites should be undertaken to determine whether different connectivity or deformation modes can further enhance composite performance under static and cyclic loading.

CRediT authorship contribution statement

Zhaozheng Meng: Writing – review & editing, Writing – original draft, Visualization, Software, Methodology, Investigation, Formal analysis, Data curation, Conceptualization. **Yading Xu:** Writing – review & editing, Methodology, Investigation, Formal analysis, Conceptualization. **Wen Zhou:** Writing – review & editing, Investigation, Formal analysis, Data curation. **Jinbao Xie:** Writing – review & editing, Software, Investigation, Formal analysis. **Branko Šavija:** Writing – review & editing, Supervision, Resources, Project administration, Methodology, Investigation, Funding acquisition, Formal analysis, Conceptualization.

Declaration of competing interest

The authors declare that they have no known competing financial interests or personal relationships that could have appeared to influence the work reported in this paper.

Acknowledgements

Zhaozheng Meng, Yading Xu, Wen Zhou, and Branko Šavija acknowledge the financial support from the European Research Council (ERC) within the framework of the ERC Starting Grant Project "Auxetic Cementitious Composites by 3D printing (ACC-3D)", Grant Agreement Number 101041342. Views and opinions expressed are however those of the author(s) only and do not necessarily reflect those of the European Union or the European Research Council. Neither the European Union nor the granting authority can be held responsible for them. Jinbao Xie would like to acknowledge the funding supported by China Scholarship Council (CSC) under the grant CSC No. 202006260045.

Data availability

Data will be made available on request.

References

[1] Shang XY, Qu N, Li JS. Development and functional characteristics of novel foam concrete. Constr Build Mater 2022;324.
[2] Wu K, Shao ZS, Qin S. A solution for squeezing deformation control in tunnels using foamed concrete: a review. Constr Build Mater 2020;257.
[3] Feng SW, Zhou Y, Li Q. Damage behavior and energy absorption characteristics of foamed concrete under dynamic load. Constr Build Mater 2022;357.
[4] Chung SY, Kim JS, Lehmann C, Stephan D, Han TS, Abd Elrahman M. Investigation of phase composition and microstructure of foamed cement paste with different supplementary cementing materials. Cement Concr Compos 2020;109.
[5] Parmigiani S, Falliano D, Moro S, Ferro GA, Restuccia L. 3D-printed multi-functional foamed concrete building components: material properties, component design, and 3D printing application. Developments in the built environment 20. 2024.
[6] Ahmad MR, Chen B, Shah SFA. Investigate the influence of expanded clay aggregate and silica fume on the properties of lightweight concrete. Constr Build Mater 2019;220:253–66.
[7] Bayraktar OY, Tunçtan M, Benli A, Türkel I, Kizilay G, Kaplan G. A study on sustainable foam concrete with waste polyester and ceramic powder: properties and durability. J Build Eng 2024;95.
[8] Yang SZ, Wang XJ, Hu ZJ, Li JW, Yao XL, Zhang C, Wu CL, Zhang JZ, Wang WL. Recent advances in sustainable lightweight foamed concrete incorporating recycled waste and byproducts: a review. Constr Build Mater 2023;403.
[9] Khan M, Shakeel M, Khan K, Akbar S, Khan A. A review on fiber-reinforced foam concrete. Engineering Proceedings 2022;22(1):13.
[10] Huang BF, Xiao Y. Compressive impact tests of lightweight concrete with 155-mm-diameter spilt hopkinson pressure bar. Cement Concr Compos 2020;114.
[11] Wang B, Chen YS, Fan HL, Jin FN. Investigation of low-velocity impact behaviors of foamed concrete material. Composer Part B-Eng 2019;162:491–9.
[12] Zhang SW, Wang R, Zhang JL, Yuan Y. Enhancing toughness in cement-based composites: unraveling the composite effect mechanisms of polymers and fibers through physic testing and molecular dynamics simulations. Compos Part B-Eng 2024:287.
[13] Tian DX, Hou JJ, Liang JK, Chen JB. Fabrication of polypropylene/carbon fiber/carbon black composite foam bonded with continuous carbon fiber reinforced polypropylene prepregs via high-pressure foam injection molding. Composer Part B-Eng 2025;291.
[14] Feng S, Gao YD, Xiao HG, Xue CH. Influence of fibers and bubble structure on thermal conductivity and mechanical performances of foam concrete. Constr Build Mater 2024;445.
[15] Li JH, Hajimohammadi A, Yu Y, Lee BY, Kim T. Mechanism of PVA fiber influence in foam concrete: from macroscopic to microscopic view. J Mater Civ Eng 2023;35(12).
[16] Gencel O, Nodehi M, Bayraktar OY, Kaplan G, Benli A, Gholampour A, Ozbakkaloglu T. Basalt fiber-reinforced foam concrete containing silica fume: an experimental study. Constr Build Mater 2022;326.
[17] Ahmad MR, Chen B. Experimental research on the performance of lightweight concrete containing foam and expanded clay aggregate. Composer Part B-Eng 2019;171:46–60.
[18] Wang XQ, Jin YL, Ma Q, Li X. Performance and mechanism analysis of natural fiber-reinforced foamed concrete. Case Stud Constr Mater 2024;21.
[19] Falliano D, De Domenico D, Ricciardi G, Gugliandolo E. Compressive and flexural strength of fiber-reinforced foamed concrete: effect of fiber content, curing conditions and dry density. Constr Build Mater 2019;198:479–93.
[20] Amran YHM, Farzadnia N, Ali AAA. Properties and applications of foamed concrete; a review. Constr Build Mater 2015;101:990–1005.
[21] Kilincarslan S, Davraz M, Isildar N. Investigation of the effect of autoclaving on foam concrete properties. J Radiat Res Appl Sc 2023;16(4).
[22] Nguyen TK, Suhaizan MS, Nguyen-Xuan H, Tran P. Mechanical responses of buoyant bio-inspired foamed concrete structures. Constr Build Mater 2023;391.
[23] Xu YD, Wan Z, Savija B. Elevating mechanical performance of cementitious composites with surface-modified 3D-Printed polymeric reinforcements. Developments in the Built Environment 2024;19.
[24] Edmund D, Zahra T, Asad M, Thamboo J. Experimental investigation on tensile characteristics of 3D printed auxetic embedded cementitious composites and shear bonding behaviour to masonry. J Build Eng 2024;97.
[25] Liu JW, Kanwal H, Tang C, Hao WF. Study on flexural properties of 3D printed lattice-reinforced concrete structures using acoustic emission and digital image correlation. Constr Build Mater 2022;333.
[26] Xu LH, Yang Z, Zhang ZL, Li E, Zhou J, Li B. Lightweight composite meta-lattice structures with inertial amplification design for broadband low-frequency vibration mitigation. Compos Part B-Eng 2025;292.
[27] Momoh EO, Jayasinghe A, Hajsadeghi M, Vinai R, Evans KE, Kripakaran P, Orr J. A state-of-the-art review on the application of auxetic materials in cementitious composites. Thin-Walled Struct 2024;196.
[28] Xu Y, Šavija B. Auxetic cementitious composites (ACCs) with excellent compressive ductility: experiments and modeling. Mater Des 2024;237.
[29] Hassani F, Javanbakht Z, Malek S. Large deformation behavior and energy absorption of rotating square auxetics. Compos Part B-Eng 2024;283.
[30] Choudhry NK, Panda B, Kumar S. In-plane energy absorption characteristics of a modified re-entrant auxetic structure fabricated via 3D printing. Composer Part B-Eng 2022;228.
[31] Grima JN, Alderson A, Evans KE. Auxetic behaviour from rotating rigid units. Phys Status Solidi B 2005;242(3):561–75.
[32] Zhang Y, Ren X, Jiang W, Han D, Zhang XY, Pan Y, Xie YM. In-plane compressive properties of assembled auxetic chiral honeycomb composed of slotted wave plate. Mater Des 2022;221.
[33] Zahra T, Dhanasekar M. Characterisation of cementitious polymer mortar - auxetic foam composites. Constr Build Mater 2017;147:143–59.
[34] Ren X, Das R, Tran P, Ngo TD, Xie YM. Auxetic metamaterials and structures: a review. Smart Mater Struct 2018;27(2).
[35] Mizzi L, Attard D, Evans KE, Gatt R, Grima JN. Auxetic mechanical metamaterials with diamond and elliptically shaped perforations. Acta Mech 2021;232(2):779–91.
[36] Zhang Y, Jiang WZ, Jiang W, Zhang XY, Dong J, Xie YM, Evans KE, Ren X. Recent advances of auxetic metamaterials in smart materials and structural systems. Adv Funct Mater 2025:2421746.
[37] Liu B, Feng JW, Yu K, Li JQ, Hu QR, Lin ZW, Fu JZ. Three-dimensional auxetic structure design methods based on bulking-induced deformation and the application in soft crawling robot. Composer Part B-Eng 2022;244.
[38] Xue YY, Wang W, Han FS. Enhanced compressive mechanical properties of aluminum based auxetic lattice structures filled with polymers. Composer Part B-Eng 2019;171:183–91.
[39] Li TT, Liu F, Wang LF. Enhancing indentation and impact resistance in auxetic composite materials. Compos Part B-Eng 2020;198.
[40] Chen M, Yao XH, Zhu L, Yin MS, Xiong Y, Hu N. Geometric design and performance of single and dual-printed lattice-reinforced cementitious composite. Cement Concr Compos 2023;143.
[41] Jiang W., Ren X., Wang S.L., Zhang X.G., Zhang X.Y., Luo C., Xie Y.M., Scarpa F., Alderson A., Evans K.E. Manufacturing, characteristics and applications of auxetic foams: a state-of-the-art review. Compos Part B-Eng 2022;235.
[42] Asad M, Win N, Zahra T, Thambiratnam DP, Chan THT, Zhuge Y. Enhanced energy absorption of auxetic cementitious composites with polyurethane foam layers for building protection application. J Build Eng 2023;78.
[43] Chen M, Chen Z, Xuan Y, Zhang T, Zhang M. Static and dynamic compressive behaviour of 3D printed auxetic lattice reinforced ultra-high performance concrete. Cement Concr Compos 2023;139.
[44] Choudhry NK, Nguyen TK, Nguyen-Van V, Panda B, Tran P. Auxetic lattice reinforcement for tailored mechanical properties in cementitious composite: experiments and modelling. Constr Build Mater 2024;438.
[45] Xie BL, Tian RT, Zhao HY, Ye TT, Zhang Y, Hu N. Controlling crack propagation in layered beams with architected lattice-reinforced composite interlayer designs. Constr Build Mater 2024;426.
[46] Vitalis T, Gross A, Tzortzinis G, Schagen B, Gerasimidis S. Enhancing mortar composite matrices with three-dimensional auxetic truss lattice materials for reinforced concrete structures. Constr Build Mater 2024;457.
[47] Tzortzinis G, Gross A, Gerasimidis S. Auxetic boosting of confinement in mortar by 3D reentrant truss lattices for next generation steel reinforced concrete members. Extreme Mech Lett 2022;52.
[48] Meng ZZ, Xu YD, Xie JB, Zhou W, Bol RJM, Liu QF, Savija B. Unraveling the reinforcing mechanisms for cementitious composites with 3D printed multidirectional auxetic lattices using X-ray computed tomography. Mater Des 2024;246.
[49] Li X, Peng WT, Wu WW, Xiong J, Lu Y. Auxetic mechanical metamaterials: from soft to stiff. Int J Extreme Manuf 2023;5(4).
[50] Ren X, Shen JH, Ghaedizadeh A, Tian HQ, Xie YM. A simple auxetic tubular structure with tuneable mechanical properties. Smart Mater Struct 2016;25(6).
[51] Wang K, Chang YH, Chen YW, Zhang C, Wang B. Designable dual-material auxetic metamaterials using three-dimensional printing. Mater Des 2015;67:159–64.
[52] Xu Y, Meng Z, Bol RJM, Šavija B. Spring-like behavior of cementitious composite enabled by auxetic hyperelastic frame. Int J Mech Sci 2024;275.
[53] Lim T-C. A partially auxetic metamaterial inspired by the Maltese cross. Cambridge: Cambridge University Press; 2022.
[54] Mukhopadhyay T, Kundu D. Mixed-mode multidirectional Poisson's ratio modulation in auxetic 3D lattice metamaterials. Adv Eng Mater 2022;24(5).
[55] Tretiakov KV, Wojciechowski KW. Auxetic, partially auxetic, and nonauxetic behaviour in 2D crystals of hard cyclic tetramers. Phys Status Solidi-R 2020;14(7).